JMEPEG (2007) 16:461–469
DOI: 10.1007/s11665-007-9041-3

1059-9495/$19.00

A Mathematical Model to Predict Microstructure of Heat-Treated Steel

V.K. Sinha, R.S. Prasad, A. Mandal, and J. Maity

(Submitted February 22, 2006; in revised form May 9, 2006)

The dual effects of chemical composition and cooling rate on microstructural evolution were theoretically simulated extending the Johnson-Mehl equation for non-isothermal pro-eutectoid ferrite transformation kinetics incorporating the effect of supercooling (ΔT) as well as for isothermal pearlite transformation kinetics assuming the exponent on time 'n' to vary inversely with time as, $n = p/t^m$, for case carburized steel quenched in oil. Carbon concentration profile of steel carburized at 930 °C for 10 h was theoretically computed by solving the Fick's diffusion equation. The cooling curves from surface to core were generated for typical 20.32 and 15.6 mm diameter steels using FEM package (ANSYS) for oil quenching, water quenching, and air cooling. The effect of varying carbon concentration from surface to core was incorporated in the heat transfer equations while generating cooling curves, at different case depths (surface, 0.31, 0.558, 1.239, and 3.469 mm). The cooling curves for oil quenching were superimposed on the published TTT diagrams of the steels of corresponding carbon content and using the empirical equations the evolution of different microconstituents, e.g., ferrite, pearlite, and martensite from the parent austenite phase were computed for the carburized 20.32 and 15.6 mm diameter steel samples. These steel samples were also case carburized experimentally at 930 °C for 10 h followed by oil quenching. The theoretically predicted case depth of 3.469 mm matched closely with the experimentally observed value. Microstructural studies were done on inverted microscope and quantitative image analyzer at different case depths/nodal points. Microhardnesses were also measured at case depths from 0.1 mm to center of the samples at selected areas to identify the different phases. The experimentally observed microstructures matched well with the theoretically predicted evolution of microconstituents.

Keywords Mathematical Model, Carbon Steel, Carburization, Diffusion, Quenching, Heat Transfer, FEM Package, ANSYS, Cooling Curves, Phase Transformation, TTT Diagram, Case Depth, Metallographic Characterization

1. Introduction

The phase transformation in steels during heat treatment leading to evolution of microconstituents such as ferrite, pearlite (eutectoid mixture of ferrite and cementite), bainite (mixture of supersaturated ferrite and epsilon-carbide) and martensite is dependent on chemical composition and cooling rate. The type, amount and morphology of the microconstituents in the heat-treated steels determine their mechanical properties. Considerable amount of work has been done to determine the microstructures of heat-treated steels experimentally and results are published by plotting the phase diagrams and isothermal transformation or time-temperature-transformation (TTT) diagrams (Ref 1). Experimental generation of such data are both time consuming and expensive. Keeping this in view several attempts have been made in the recent past (Ref 2-5) to theoretically predict the microstructural evolution in micro-alloyed, dual phase, and trip steels of high strength to weight ratio. Case carburized steel is an important system where the carbon concentration varies with case depth and so is the cooling rate during quenching. Therefore both the effect of cooling rate and chemical composition can be predicted on the microstructural evolution in steel during its heat treatment. However only a few data are available in the literature for microstructural simulation in case carburized hardened steels.

In the present investigation; therefore, a theoretical model was developed using the FEM package (ANSYS) generating cooling curves for oil quenching, water quenching, and air cooling at different case depths of the carburized steels of diameter 20.32 and 15.6 mm, respectively. Typical cooling curves obtained for oil quenching were superimposed on the published TTT diagrams to simulate the microstructural evolution by incorporating the effect of supercooling (ΔT) and assuming the exponent on time 'n' to vary inversely with time as, $n = p/t^m$ in the Johnson-Mehl equation for case carburized steel quenched in oil. Microstructural studies and microhardness measurement of 20.32 and 15.6 mm diameter steel samples experimentally carburized at 930 °C for 10 h followed by oil quenching are also included in the present investigation. The theoretically predicted and experimentally observed microstructures are compared.

V.K. Sinha and **J. Maity,** Department of Materials and Metallurgical Engineering, National Institute of Foundry & Forge Technology, Hatia, Ranchi 834003, Jharkhand, India; **R.S. Prasad,** Foundry & Forge Technology, National Institute of Foundry and Forge Technology, Hatia, Ranchi 834003, Jharkhand, India; **A. Mandal,** Department of Manufacturing Engineering, National Institute of Foundry and Forge Technology, Hatia, Ranchi 834003, Jharkhand, India. Contact e-mail: sinhavijay46@rediffmail.com.

2. Theoretical Modeling

2.1 Concentration Profile in the Carburized Sample

The solution to Fick's second law under the boundary conditions $C = C_0$ at $t = 0$, $0 < x < \infty$ and $C = C_s$ at $x = 0$, $0 < t < \infty$ is given by (Ref 6)

$$[(C_x - C_s)/(C_0 - C_s)] = \text{erf}[x/(2 \times (D \times t)^{1/2})] \quad \text{(Eq 1)}$$

where, $C(x, 0) = C_0$ (here C_0 = 0.2 %Carbon), $x > 0$; $C(0, t) = C_s$ (here C_s = 0.8 %Carbon), C_x is the carbon concentration (in weight percentage) at a distance x from the surface, D = diffusion co-efficient of carbon in γ-iron, t = time (here t = 10 h = 36,000 s),

The diffusion coefficient of carbon in γ-iron is

$$D = D_0 \exp(-Q/RT) = 1.066 \times 10^{-11}\ \text{m}^2/\text{s} \quad \text{(Eq 2)}$$

where D_0 is a pre-exponential constant and Q is the activation energy for diffusion with computed values, $D_0 = 0.7 \times 10^{-4}$ m^2/s (for carbon in γ-iron), $Q = 157 \times 10^3$ J/mol (for carbon in γ-iron), T = carburizing temperature = 930 °C = 1203 K, R = gas constant = 8.314 J/mol per Kelvin The carbon concentration at the different nodal points were computed from the Fick's diffusion equation 1.

2.2 Generation of Cooling Curve by using FEM Package (ANSYS)

The following assumptions were made for developing the model:

(i) Considered very long cylindrical rod (length to diameter ratio > 5) and heat transfer along length was neglected.
(ii) Two dimensional heat transfer equation was solved by using FEM) Package (ANSYS), considering that heat transfer takes place along radial direction only.
(iii) Since after carburization the carbon content varied from surface toward center till certain depth along the radius (i.e., till case depth) and it remained constant in core, the modeling was done by using one solid circle and four annuluses. Core (0.2%C) was represented by the solid circle. Carburized case was represented by four annuluses. Nodal points (G, F, E, D, C) were set at the periphery of each annulus and solid circle for carburized case. Two additional nodal points (B, A) were also considered inside the core including center. The carbon content at different nodal points were computed from Eq 1. Selection of nodal points with respect to distance from surface and carbon content are summarized in Table 1. The nodal points are shown in Fig.1. Cooling curves were generated for all nodal points.
(iv) Constant effective film co-efficient was considered (Ref 7), as given in Table 2.
(v) Temperature and composition dependent thermal conductivity were used by considering the following equation (Ref 8)

$$K = a - bW + c\,W^2 \quad \text{(Eq 3)}$$

where K = thermal conductivity, W/m·°C; $a = 76.8 - 6.68 \times 10^{-2}$(T); $b = 34.2 - 9.9 \times 10^{-2}(T) + 0.815 \times 10^{-4}(T)^2$; $c = 9.31 - 3.96 \times 10^{-2}(T) + 0.418 \times 10^{-4}(T)^2$; W = total amount of alloying elements, weight percentage.

Table 1 Selection of nodal points

Specimen diameter, mm	Nodal points	Distance from surface, mm	% Carbon
20.32	G	0.00 (Surface)	0.8
	F	0.31	0.6
	E	0.558	0.5
	D	1.239	0.3
	C	3.469	0.2
	B	5.96	0.2
	A	10.16 (Center)	0.2
15.6	G	0.00 (Surface)	0.8
	F	0.31	0.6
	E	0.558	0.5
	D	1.239	0.3
	C	3.469	0.2
	B	5.06	0.2
	A	7.8 (Center)	0.2

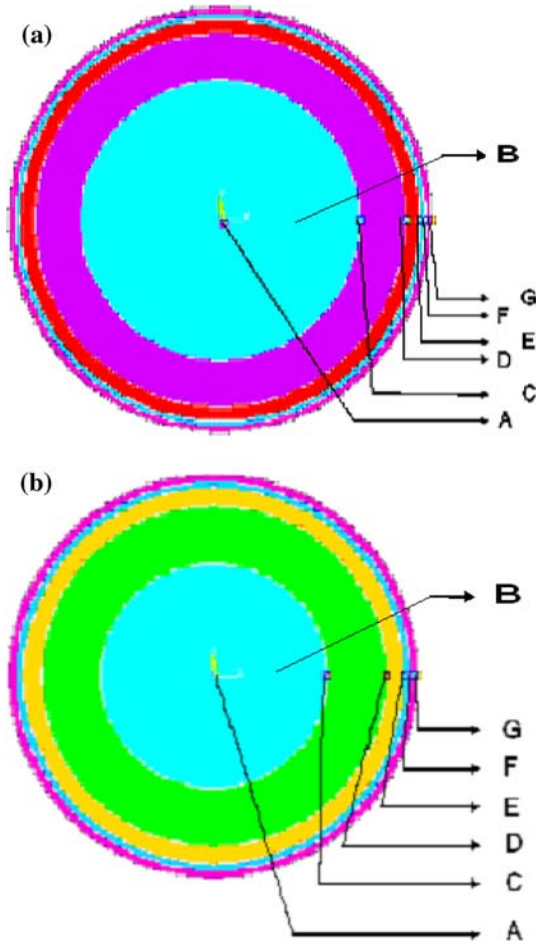

Fig. 1 Location of nodal points on the carburized steel specimens, (a) 20.32 mm Diameter, (b) 15.6 mm Diameter

Specific enthalpy (i) values considered for present work (Ref 8) and calculated thermal conductivity (K) are summarized in Table 3.

ANSYS generated cooling curves are shown in Fig. 2.

Table 2 Data for selected quenchants

Quenchant	Temperature, °C	Speed, m/s	Effective film co-efficient, h·W/m²·K
Conventional Oil	65	0.51	3000
Water	32	0.51	12,000
Air	27	–	300

2.3 Semi-theoretical Simulation of Microstructure in as Quenched Carburized Steel

The generated cooling curves from surface to center at different nodal points were superimposed on published TTT (time-temperature-transformation) diagrams of plain carbon steel of corresponding carbon content to find variation in microstructure. During calculation, in all TTT diagrams transformation-start and transformation-finish were considered as 0.01 and 0.99 fraction transformed, respectively.

2.3.1 Calculation of Pro-eutectoid Ferrite formed. Assuming that a constant rate of nucleation (I) occurs randomly in the untransformed phase (austenite) and that the product particle (ferrite) grow at a constant rate (U) as spheres, till impingement with neighboring particles occurs, the fraction of ferrite transformed (x) isothermally as a function of time (t) is given by Johnson-Mehl equation (Ref 9),

$$x = 1 - \exp(-(\pi/3) \times I \times U^3 \times t^4) \quad \text{(Eq 4)}$$

In the present work, the Johson-Mehl equation was extended for non-isothermal pro-eutectoid ferrite transformation kinetics during continuous cooling by incorporating degree of super cooling (ΔT). Accordingly:

$$\ln(1-x) = -A \times t^4 \times \exp[-B/\{(\Delta T)^2 \times T\}] \quad \text{(Eq 5)}$$

where x = fraction of pro-eutectoid ferrite formed at time t and absolute temperature T, $\Delta T = (T_{fe} - T)$ and T_{fe} = Pro-eutectoid ferrite transformation-start temperature at equilibrium.

The Eq 5 was generated considering the following fundamental relationships:

$$I \propto \exp[-(\Delta f^* + \Delta H_d)/RT] \quad \text{(Eq 6)}$$

$$\Delta f^* \propto 1/(\Delta T)^2 \quad \text{(Eq 7)}$$

where, Δf^* = the nucleation barrier; ΔH_d = the activation barrier for diffusion across interface; R = the molar gas constant.

In the present case, ΔH_d was ignored since at higher transformation temperature, viz., $T \geq$ nose temperature (i.e., temperature of our interest), $\Delta f^* \ggg \Delta H_d$ and U (which mainly depends on ΔH_d) was assumed constant. The constant 'A' in Eq 5 contains terms like, growth rate (U),π, frequency ($v \approx$ Debye frequency), etc., which may be considered constant and independent of carbon content. The constant 'B' in Eq 5 contains terms like, activation energy for diffusion (ΔH_d), enthalpy of transformation, transformation temperature, etc., which to first approximation in narrow temperature interval may also be considered constant and independent of carbon content. The CCT diagrams at carbon concentration of nodal points are barely available in the literature, whereas the TTT diagrams are readily available. A simplified model of first approximation was, therefore, developed for gross transformation characteristics in the present work. A more refined model using CCT data would be considered in due course of time and the results would be published separately. Accordingly, to find two unknowns A and B of Eq 5 the cooling curve at center of 20.32 mm diameter specimen superimposed on corresponding TTT (of 0.2%C steel) diagram was considered (Fig. 3). The known data points a1(point of intersection between pro-eutectoid ferrite start curve and the cooling curve) and b1 (point of intersection between 50% pro-eutectoid ferrite transformation curve and cooling curve) were used to find out two unknown constants A and B of Eq 5. The values of A and B were computed to be 0.008987 and 6,502,600, respectively. The Eq 5, with same value of A and B, was used to calculate % of pro-eutectoid ferrite at all the nodal points of both specimens. Total amount of pro-eutectoid ferrite formed was found out corresponding to the data point where cooling curve intersected pearlite, start curve (for e.g., data point c1 in Fig. 3). It was assumed that once pearlitic transformation started no further pro-eutectoid ferrite formation was possible.

2.3.2 Calculation of Pearlite formed. For the cooling curves intersecting pearlite-finish curve above nose, fraction of pearlite formed was calculated as (1—fraction of pro-eutectoid ferrite formed). No martensite formed in this case.

Since near and below the nose the TTT and the CCT curves more or less overlap and since pearlitic transformation occurred in a narrow temperature interval in the oil quenched samples, isothermal pearlite transformation was considered to occur. Thus when cooling curve passes between pearlite-start nose and

Table 3 Calculated Value of *K* and *i* (Ref 8)

	0.2 %C		0.3 %C		0.5 %C		0.6 %C		0.8 %C	
Temp., Kelvin	*K*	*i*	*K*	*i*	*K*	*i*	*K*	*i*	*K*	*i*
673	43	216,040	42.27	214,360	40.81	214,365	40.09	216,040	38.65	219,390
773	38.57	280,520	38.05	279,470	35.55	279,990	36.50	281,560	35.46	284,700
873	33.34	354,200	33.05	351,690	32.49	351,065	32.23	352,950	31.75	356,720
973	27.32	439,610	27.25	432,280	27.25	427,155	27.28	429,350	27.52	433,750
1073	20.51	562,710	20.66	550,980	21.28	547,630	21.66	556,000	22.76	572,750
1203	10.46	651,760	10.92	630,340	12.44	620,610	13.33	632,300	15.59	655,680

Unit of '*K*' is 'W/m · °C' and '*i*' is 'J/kg'

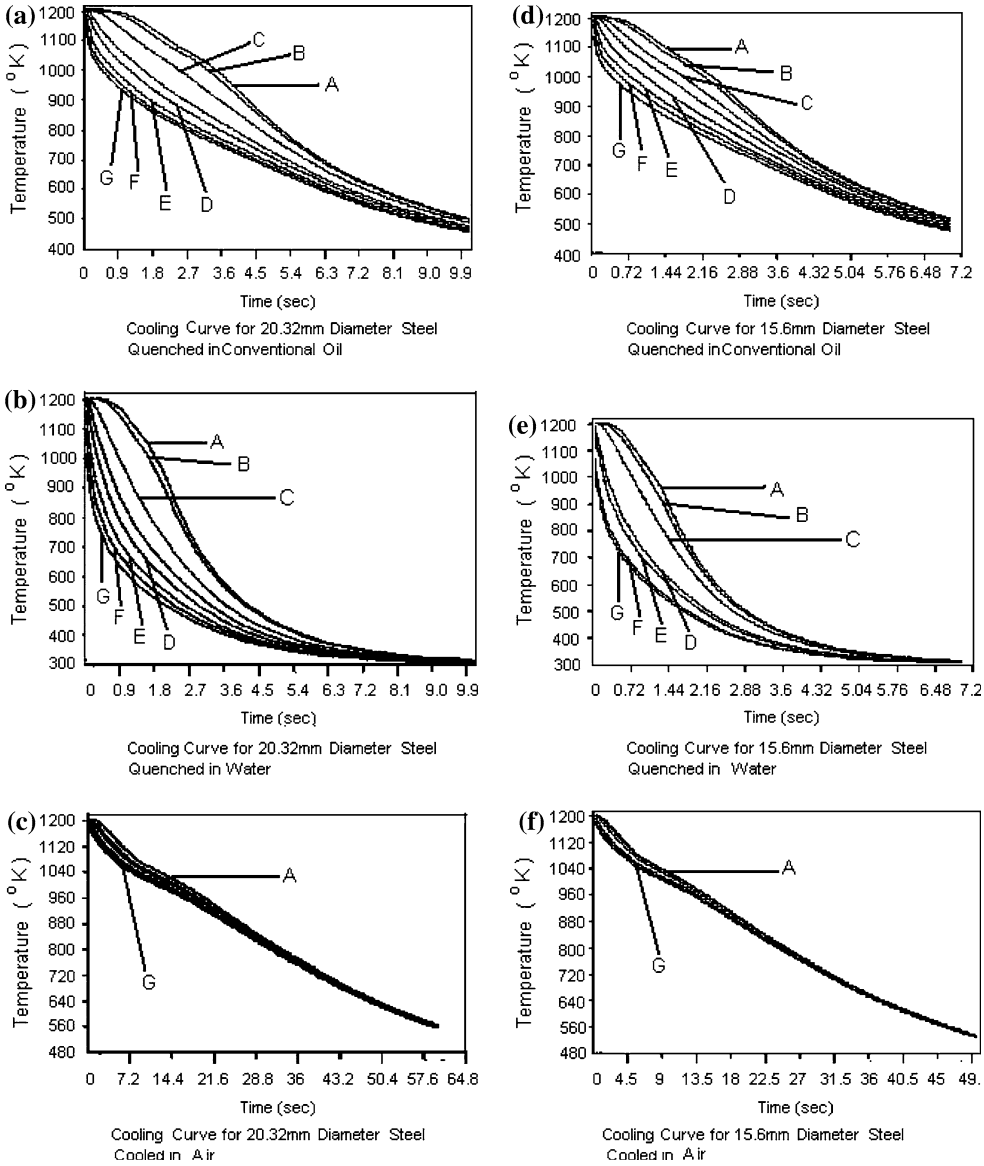

Fig. 2 Cooling curves for 20.32 and 15.6 mm diameter steel specimens in different quenching media

pearlite-finish nose, pearlitic transformation using TTT diagram is supposed to be determined as the percentage pearlite transformed corresponding to the particular C-curve of pearlitic transformation whose nose was passed through by a particular cooling curve pertaining to a particular nodal point. In present model it was considered that this point of intersection between the nose of a particular C-curve and the cooling curve was also the point of intersection between the cooling curve and the horizontal isothermal transformation line at nose temperature. The amount of pearlite formed was calculated accordingly. In order to perform such calculation, isothermal pearlitic transformation equations were generated at nose temperature in the following manner:

The progress of isothermal pearlitic transformation at nose temperature was considered to follow the following empirical equation:

$$F = 1 - \exp(-K_1 \times t^n) \quad \text{(Eq 8)}$$

where, F is the fraction of pearlite formed in time t. Equation 8 is similar to Johnson-Mehl (Ref 9) and Avrami (Ref 10) equation for isothermal pearlite transformation with the modification that unlike the exponent on time 'n' assuming a value between 3 and 4 for spherical nuclei considering nucleation rate to be constant (Ref 9) or dependent on time (Ref 10), the same was assumed in the present work to be an empirical variable dependent on time. Further, since in reality, transformation slows down with time the exponent 'n' was assumed to vary inversely with time as, $n = p/t^m$. Neglecting higher order terms of the exponential series in Eq 8, $F = K_1 \times t^n$. Thus, $\ln F = \ln K_1 + n \ln t$, or $\ln F = \ln K_1 + (p/t^m) \times \ln t$. As an illustrative example, for node G (0.8% C), the following data were retrieved from the TTT diagram and the cooling curve for 15.6 mm dia case carburized steel (Fig. 4): Nose temperature, (T_N) = 538 °C, for $F = 0.01$, $t = 0.814$ s, and for $F = 0.99$, $t = 5.45$ s. The value of m was selected as 0.66 after several trials. Accordingly, at nodal point G (0.8%C) it was derived

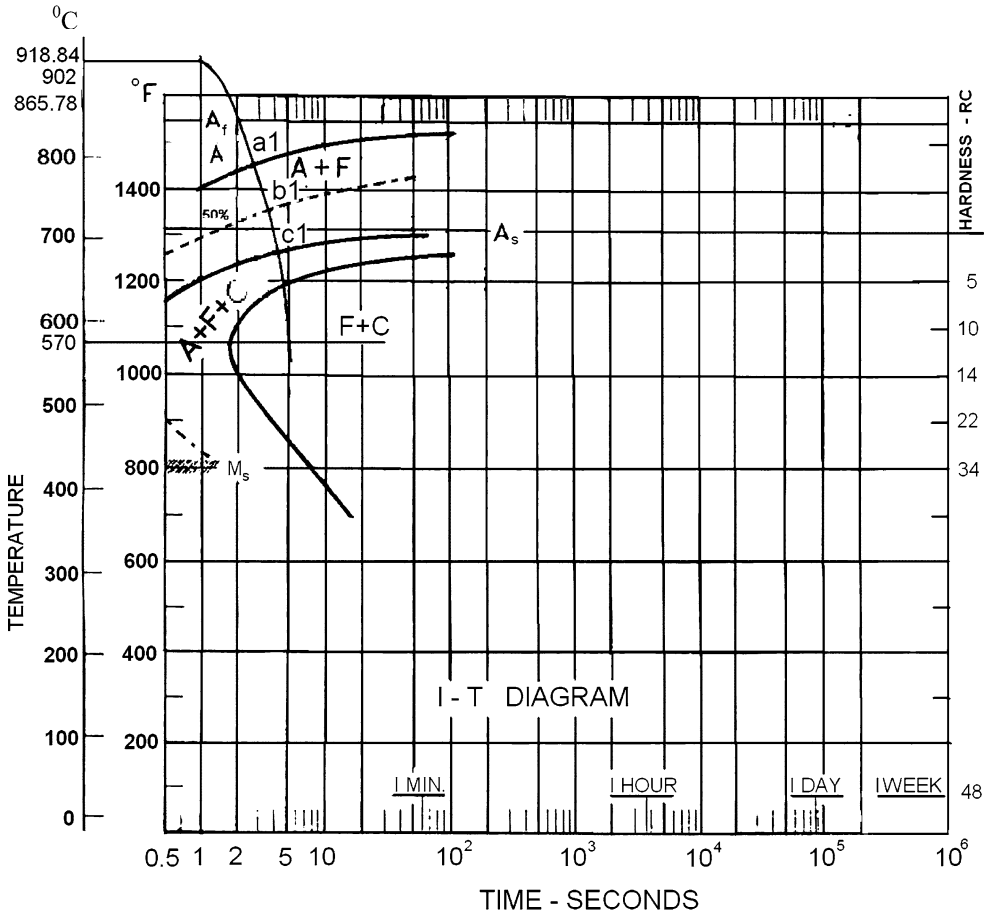

Fig. 3 Superimposition of cooling curves at center for 20.32 mm diameter specimen (Carburized & Quenched in Oil) on TTT diagram of 0.2% carbon steel (Ref 1)

that $F = 1-\exp(-0.03935 \times t^n)$, where $n = 5.8239/t^{0.66}$. The fraction of austenite transformed to pearlite after 2.39 s [the time of intersection of the cooling curve at T_N (538 °C)] was thus computed to be 0.495 in good agreement with the experimental value. The values of K_1, p, and m are supposed to vary with carbon content (different TTT diagrams). Therefore, for different carbon content (different TTT diagrams) the values of K_1, p, and m were separately calculated by interpolating to nearest known (t, F) data points around the point of intersection and through trial and error along the isothermal transformation line. Accordingly isothermal pearlitic transformation equations were generated at nose temperature for different carbon content (Table 4).

2.3.3 Calculation of Martensite formed. The fraction of the martensite formed was computed from the relation,

$$\text{Fraction of martensite formed} = [1 - (\text{fraction ferrite} + \text{fraction pearlite})] \quad \text{(Eq 9)}$$

The theoretically calculated %ferrite, %pearlite, and %martensite are graphically shown in Fig. 5.

3. Experimental Procedure

Plain carbon steel bars with length to diameter ratio 8 (in concurrence with theoretical modeling) of 20.32 and 15.6 mm diameter were used for case carburization. The results of chemical analysis of the above steel bars obtained on a direct reading spectrometer (SPECTRO, LAB JR-CCD, GERMANY) are summarized in Table 5. The base steel bars were annealed at 900 °C for microstructural study in the uncarburized condition.

The 20.32 and 15.6 mm diameter bars were packed with a mixture of 20% barium carbonate and 80% graphite and coal mixture powder (in 1:4 ratio) in a cylindrical carburizing jar made by electric arc welding a circular plate (130 mm diameter and 4 mm thickness) at one end of the truncated circular pipe (inner diameter 101.6 mm, outer diameter 109.6 mm and length 304 mm). The carburizing jar was put inside a muffle furnace held at 670 °C. The temperature of muffle furnace was subsequently increased to 930 °C. After the temperature reached 930 °C the start of soaking time was recorded. The samples were carburized at 930 °C ± 2 °C for 10 h (Ref 11) and then pulled out and quenched for 2 min in the quenching oil. As quenched carburized steel specimens were cut from the middle of the bar and were studied under inverted projection microscope (NIKON, JAPAN) and quantitative image analyzer (SELWA OPTICAL, JAPAN) from surface to center across the cross section at nodal points. The different phases regions, e.g., ferritic, pearlitic, and martensitic were further identified by microhardness testing (ERNST LEITZ WETZLAR GMBH microhardness tester) using 50 gm load (400 ×) at nodal points on different phases. In addition to the quantitative image

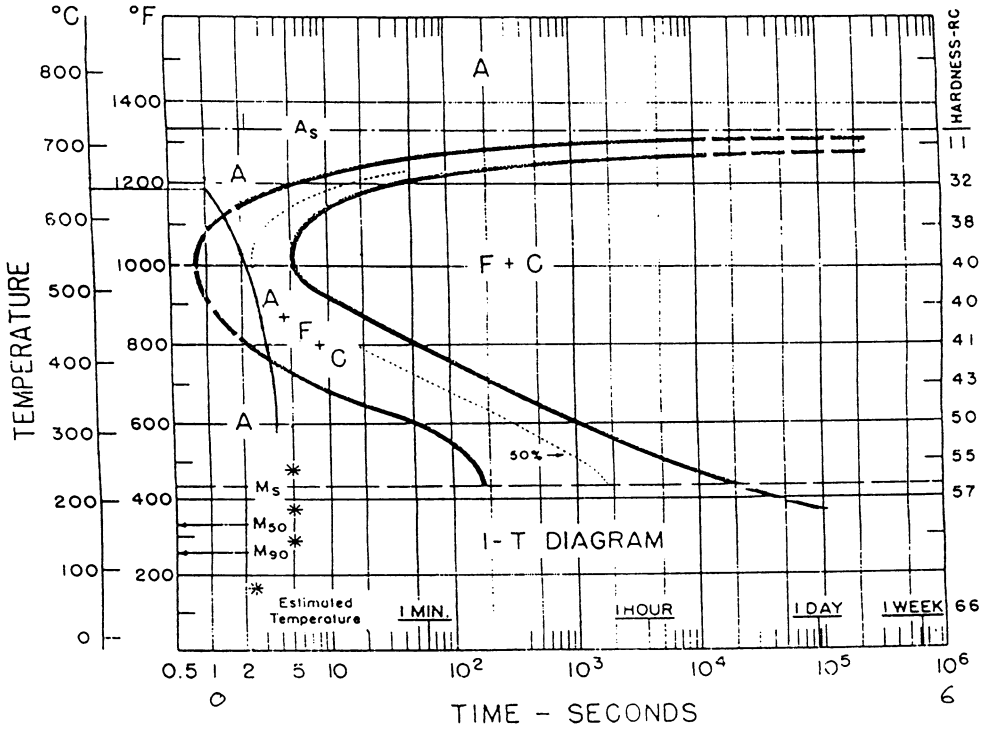

Fig. 4 Cooling curve at surface (node G) of 15.6 mm diameter carburized and oil quenched specimen superimposed on corresponding TTT diagram of 0.8% carbon steel (Ref 1)

Table 4 Pearlitic transformation equations

%Carbon	Pearlitic transformation equation
0.8	$F = 1-\exp(-0.03935\times t^n)$; where, $n = 5.8239/t^{0.66}$
0.6	$F = 1-\exp(-0.2316\times t^n)$; where, $n = 1.8027/t^{0.45}$
0.5	$F = 1-\exp(-0.04795\times t^n)$; where, $n = 7.9337/t^{0.92}$
0.3	Not Required
0.2	Not Required

analysis and microhardness data, the graphical point count method on the micrographs at different nodal points were also carried out for determining fraction of ferrite, pearlite, and martensite. One sample each from the carburized and oil quenched bars of 20.32 and 15.6 mm diameter were also annealed (900 °C, 20 min) for microstructural studies on quantitative image analyzer to determine the fraction of ferrite and pearlite at various case depths.

4. Results and Discussion

The microstructure of base steel bars (20.32 and 15.6 mm diameter) which were annealed at 900 °C showed the structure of typical low carbon steel in agreement with the chemical analysis results of the steel samples. The equilibrium carbon concentration at varying case depths from the data of area fraction of pearlite (transformed austenite), using lever rule of mass conservation made for the carburized oil quenched and subsequently annealed samples of 15.6 and 20.32 mm diameter steel, matched well with theoretically predicted values obtained using Fick's diffusion equation 1. The case depth (carbon diffusion distance from the surface) of 3.469 mm obtained from Eq 1 also matched closely to the experimentally observed value. A good match between the theoretical and experimental case depths reinforced the validity of the Fick's diffusion equation for plain carbon steel and that 20 min annealing apparently did not have significant effect on carbon concentration. However, as discussed earlier, carbon contents at the nodal points used in the analysis were those computed from the Fick's diffusion equation 1. The microstructure of as quenched carburized steel specimens indicated nearly 50% pearlite and 50% martensitic structure at the nodal point G(surface) where pearlite appeared to have nucleated at the austenite grain boundaries prior to martensitic transformation. The results were observed to be as expected because the austenite had a grain growth during carburization at 930°C and therefore the preferred heterogeneous sites were available at the grain boundaries of the austenite. The microstructure at nodal points F and E exhibited small (3-8%) transformation of austenite to ferrite at the grain boundaries of austenite and within the austenitic grains which occurred prior to the pearlite transformation. Microstructure also exhibited near 40-60% of pearlitic transformation along the austenitic grain boundary and martensitic transformation was observed in the austenitic grains. Nital or Pickrol etching did not exhibit considerable variation in the gray level of the ferrite and martensite as both appeared white. Therefore, these two phases were determined quantitatively in the image analyzer also considering their shape and morphology. Microhardness testing clearly indicated, which regions were martensite and which regions were ferrite. The hardness of the martensite at the nodal points G, F, and E were observed to be 985HV, 985HV, and 965HV respectively. The reduced hardness of the martensite with increasing distance from the case hardened surface was attributed to decreasing

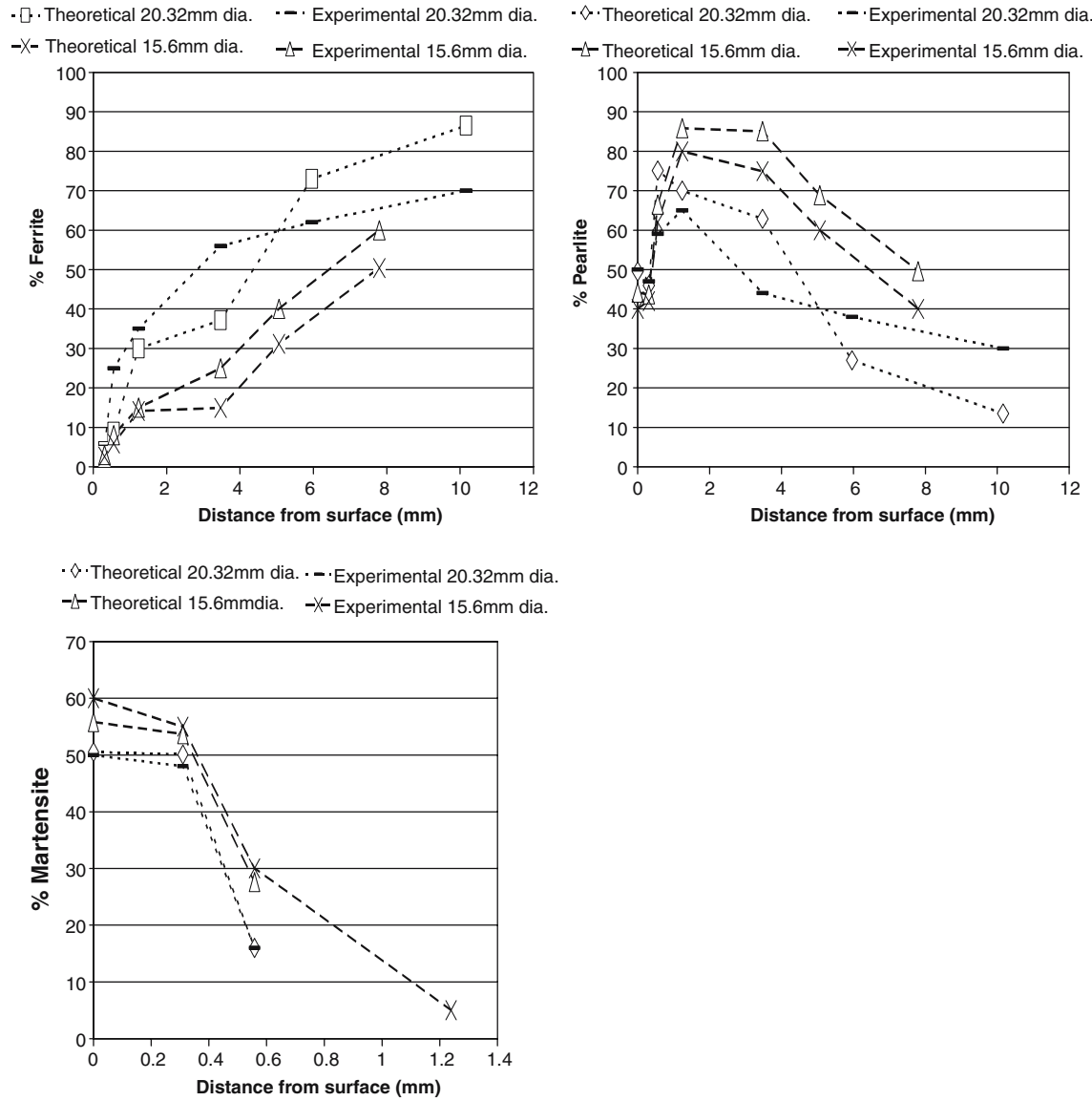

Fig. 5 Variation in %Ferrite, %Pearlite, %Martensite from surface towards center

Table 5 Chemical composition of steel specimens

Bar dia., mm	%C	%Si	%Mn	%P	%S	%Ni
20.32	0.16	0.023	0.68	< 0.0014	0.028	0.051
15.6	0.20	0.22	0.82	< 0.0014	0.023	0.032

carbon content of the martensite. The microhardness of ferrite and pearlite regions lied in the range 244HV to 221HV and 441HV to 354HV respectively. The decreasing hardness of the pearlite with increasing case depth was attributed to the coarseness of the pearlite at the interior nodal points due to decreasing cooling rate. The microhardness measurement ascertained that austenite transformed to ferrite and pearlite only without any martensitic transformation at nodal points C, B, and A in 15.6 mm diameter sample as well as at nodal points C, B, and A in 20.32 diameter sample. In addition to the quantitative image analysis and microhardness data, the graphical point count method on the micrographs at different nodal points were also used for determining fraction of ferrite, pearlite and martensite. Typical micrographs indicating the different phases obtained on image analyzer for the 20.32 mm diameter case hardened (carburized and oil quenched) sample at nodal points G, F, E, D, C, and A are shown in Fig. 6. In comparison with theoretically calculated values, the percentage of different microconstituents determined by image analysis and considering their morphology and microhardnesses are graphically plotted in Fig. 5. The quantitatively measured percentage of microconstituents, e.g., martensite, ferrite, and pearlite obtained experimentally matched considerably well (within 10-15%) to those predicted by our theoretical model of first approximation. The variation between the theoretically predicted microstructural evolution and the experimentally observed one may be primarily attributed to factors, such as, simplified boundary conditions of heat transfer, use of TTT data instead of CCT data for determining constants of the empirical equations and other simplified assumptions.

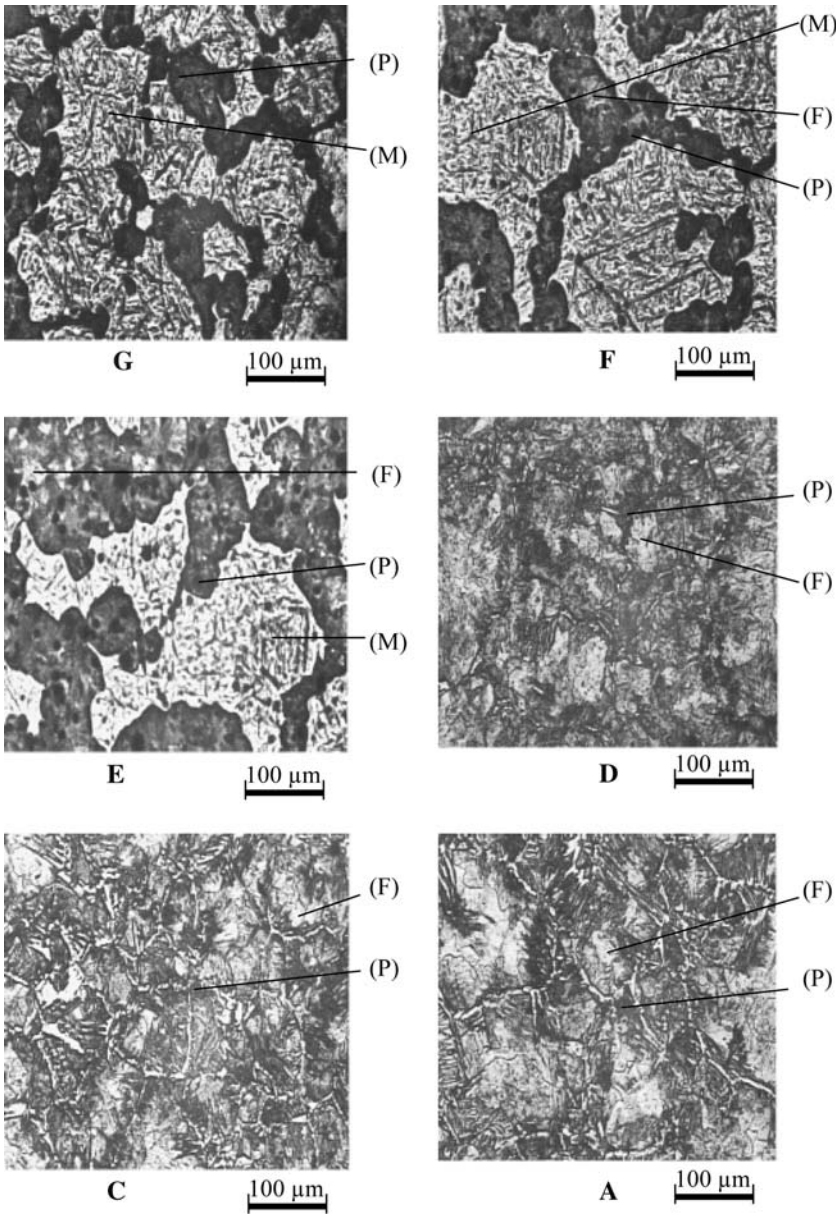

Fig. 6 Microstructure of carburized and oil quenched specimen of 20.32 diameter at different nodal points, Ferrite (F); Pearlite (P); Martensite (M)

5. Conclusions

Integrating FEA and physical metallurgy a simplified model was developed in the present work to predict microstructural evolution in case hardened plain carbon steel as a function of composition (carbon content) and cooling rate. The model was developed using FEA (ANSYS) generated cooling curves and extending the isothermal transformation equation of Johnson-Mehl for non-isothermal transformation during continuous cooling. This was done by incorporating supercooling (ΔT) in the mathematical equation. In addition the exponent 'n' was considered to be an empirical variable of time instead of its Johnson-Mehl value between 3 and 4. The experimentally observed microstructural evolution matched considerably well (within 10% to 15%) with those predicted by our theoretical model of first approximation.

References

1. Anon, *Atlas of Isothermal and Cooling Transformation Diagram*. ASM, Metals Park, Ohio, 1977, p 5–37
2. M. Hillert and L. Hoglund, Comments on – Reply to Comments on Kinetics Model of Isothermal Pearlite Formation in 0.4C-1.6Mn Steel, *Scripta Materialia*., 2004, **51**(1), p 77–78
3. M.Ph. Papaelias, M. Strangwood, A.J. Peyton, and L. Davis C., Effect of Microstructural Variations on Smart Inductive Sensor Measurements of Phase Transformation in Steels, *Scripta Materialia*., 2004, **51**(5), p 379–383
4. A.R. Mirak and M. Nili-Ahmadabadi, Effect of Modified Heat Treatments on the Microstructure and Mechanical Properties of Low Alloy High Strength Steels, *Mater. Sci. Technol.*., 2004, **20**, p 897–902
5. A. Taniyama, T. Tkayama, and M. Arai, Structure Analysis of Ferrite Indeformed Pearlitic Steel by Means of X-Ray Diffraction Method with Synchrotron Radiation, *Scripta Materialia*., 2004, **51**(1), p 53–58
6. A. Fick, *Pogg. Ann.*., 1855, **94**, p 59
7. C.E. Bates, Predicting Properties and Minimising Residual Stress in Quenched Steel Parts, *J. Heat Treating*., 1988, **6**, p 27–45

8. E.I. Kazantsev, *Industrial Furnaces*. **2**, Mir Publishers, Moscow, 1977, p 62–110
9. W.A. Johnson and R.F. Mehl, Reaction Kinetics in Processes of Nucleation and Growth, *Trans. AIME*., 1939, **135**, p 416–441
10. M. Avrami, Kinetics of Phase Change-III, *J. Chem. Phys.*., 1941, **9**, p 177–184
11. K.H. Prabhudev, *Handbook of Heat Treatment of Steels*. Tata McGraw Hill, New Delhi, 1992, p 298